Modelling ultrafine particle growth in a flow tube reactor

Michael S. Taylor Jr., Devon N. Higgins, and Murray V. Johnston

Department of Chemistry and Biochemistry, University of Delaware, Newark, Delaware, 19711, United States

Correspondence to: Murray V. Johnston (mvj@udel.edu)

Abstract. Flow tube reactors are often used to study aerosol kinetics. The goal of this study is to investigate how best to represent complex growth kinetics of ultrafine particles within a flow tube reactor when the chemical processes causing particle growth are unknown. In a typical flow tube experiment, one measures the inlet and outlet particle size distributions to determine a time-averaged measure of growth, which may be difficult to interpret if the growth kinetics change as particles transit through the flow tube. In this work, we simulate particle growth for secondary organic aerosol (SOA) formation that incorporates both surface- and volume- limited chemical processes to illustrate how complex growth kinetics inside a flow tube can arise. We then develop and assess a method to account for complex growth kinetics when the chemical processes driving the kinetics are not known. Diameter growth of particles is represented by a growth factor (GF), defined as the fraction of products from oxidation of the volatile organic compound (VOC) precursor that grow particles during a specific time period. Defined in this way, GF is the sum of all nonvolatile products that condensationally grow particles plus a portion of semivolatile molecules that react on or in the particle to give nonvolatile products that remain in the particle over the investigated time frame. With respect to flow tube measurements, GF is independent of wall loss and condensation sink, which influence particle growth kinetics and can vary from experiment to experiment. GF is shown to change as a function of time within the flow tube and is sensitive to factors that affect growth such as gas-phase mixing ratios of the precursors and the presence of aerosol liquid water (ALW) on the surface or in the volume of the particle. A method to calculate GF from outlet minus inlet particle diameter change in a flow tube experiment is presented and shown to accurately match GFs from simulations of SOA formation.

1 Introduction (as Heading 1)

Atmospheric aerosols have significant effects on human health and the environment, from the direct inhalation of air into our lungs to the changing composition of the atmosphere (Najjar, 2011; Thompson, 2018). Particulate matter in the atmosphere has been a focus of attention since the London Smog incident and similar events of the mid twentieth century (Bell et al., 2004). Both anthropogenic and biogenic emissions are major sources of new particle formation, whether it be through primary particle emissions or secondary formation (Després et al., 2012; Lehtipalo et al., 2018). Clusters of ambient molecules, such as ammonia, sulfuric acid, and organics with low volatility, are often sources for new particles in the 1 to 2 nm size range that are capable of spontaneously growing to larger sizes (Shrivastava et al., 2017). Once particles grow to the size range of 50-100 nm, they can act as cloud condensation nuclei (CCN) which are capable of affecting radiative forcing on the earth (Johnson

Deleted: based on

Deleted: measurements

Deleted: the

Deleted: of

Deleted:). Because a significant amount of growth must occur over the short residence time of the flow tube, precursor mixing ratios in a flow tube experiment are generally much higher than ambient values. In this study, a model of SOA growth based on condensation of nonvolatile molecules, partitioning of semivolatile molecules, and reaction of semivolatile molecules in the particle volume to produce nonvolatile dimers, is used to compare particle growth under atmospherically relevant conditions to those under typical flow tube conditions. The focus is on the diameter growth of particles in the 10 to 100 nm diameter range, where growth rates can have a substantial impact on

Deleted: of cloud condensation nuclei. In this size range,

Deleted: particle

Deleted: kinetics may apply. Modelling shows that the higher precursor mixing ratios of

Deleted: experiment cause surface-limited kinetics to be more prevalent in the flow tube than under atmospheric conditions. SOA formation is characterized by the

Deleted: yield (GY

Deleted: yield

Deleted: products

Deleted: are to

Deleted: the

Deleted: GY

Deleted: particles

Deleted: volume

Deleted: dimers. Modelling shows

Deleted: GY actually changes

Deleted: . The experimentally determined GY from the measured inlet-outlet diameter change of particles

Deleted: closely tracks the average of the time-dependent GY obtained from modelling specific chemical processes. Modelling is also used to explore the effects of seed particle size (40, 60, 80 nm dia.), phase state (deliquesced vs. effloresced), and surface state (interfacial water), as well as precursor mixing ratio, all of which are shown to substantially influence SOA formation under the conditions studied…

Deleted: from existing particulate matter

Deleted: ~

et al., 2018; Riipinen et al., 2011). Due to the many growth and removal processes involved in atmospheric particle growth, the likelihood of a nucleated particle to reach the CCN active range can vary greatly. Simulations of these processes may contain large uncertainties with respect to secondary organic aerosol (SOA) formed from biogenic emissions and the varying properties of organic aerosols in general (Pierce and Adams, 2007). In the work presented here, we explore fundamental aspects of using a flow tube to characterize particle growth by SOA formation in a size range relevant to CCN activity.

SOA formation occurs when a volatile organic compound (VOC) is oxidized in the gas phase. There are usually a wide range of oxidation products from a given VOC precursor, and these products can be classified by their volatility, a measure of the product molecule's ability to partition between the gas and particle phases or condense from the gas phase to particle phase (Bianchi et al., 2019). Low and Extremely Low Volatility Organic Compounds (LVOCs and ELVOCs) are able to condensationally grow particles, with LVOCs being limited by the Kelvin effect in small particles (<20 nm). Semivolatile organic compounds (SVOCs) are products with somewhat higher volatility, allowing them to partition between the gas and particle phases. Oxidized volatile organic compounds (OVOCs) are products too volatile to partition to the particles, though they remain available to participate in subsequent gas phase reactions. SVOCs and possibly OVOCs may contribute significantly to particle growth if they undergo multiphase reactions on the particle surface or within the particle volume to produce nonvolatile products that remain on/in the particle (Fuzzi et al., 2006; Gkatzelis et al., 2018).

SOA produced by the oxidation of biogenic VOCs contributes significantly to fine particulate matter in the atmosphere (Jimenez et al., 2009). The molecular composition of biogenic SOA encompasses several hundreds to thousands of potential products that can be formed through various pathways, making its inclusion in atmospheric models complex (Hallquist et al., 2009). Molecular analysis of biogenic SOA has shown evidence of particle-phase chemistry through detection of oligomers formed by accretion reactions, which may enhance the uptake of organic matter into a particle over what would be present from partitioning alone (Barsanti and Pankow, 2006; Tolocka et al., 2004a). The reactivity of VOC oxidation products can vary significantly owing largely to the presence of multiple functional groups (Jia and Xu, 2020; Zhou et al., 2018). For the oxidation of monoterpenes specifically, highly reactive hydroperoxide functionalities have been found on up to 50 % of product molecules (Docherty et al., 2005; Mertes et al., 2012) which are thought to be formed by an autooxidation mechanism (Bianchi et al., 2019; Crounse et al., 2013). Environmental factors such as relative humidity and temperature affect oxidation product formation, especially with respect to product molecule reactivity and volatility, while particle composition and phase state affect the multiphase processes these products may undergo (Zhang et al., 2015). By studying these processes and properties, one is able to more accurately define and understand the lifecycle and effects of SOA in climate cycles (Saha and Grieshop, 2016; Shrivastava et al., 2017).

The complexity of SOA chemistry as discussed above poses a challenge for studying particle growth with a flow tube reactor. In a flow tube experiment, seed particles and SOA precursors (VOC and oxidant) are mixed at the entrance of the flow tube,

Deleted: aerosols

Deleted: Particle growth rates are generally studied in the laboratory using either chamber or flow tube reactors. With chamber reactors, precursors are added to the (sealed) reactor at time t=0 and the evolution of particles inside the reactor is monitored as a function of time . With flow tube reactors, which are the focus of this study, precursors are mixed at the entrance of the flow tube and the product distribution of aerosol exiting the tube is monitored . Flow tubes provide the opportunity to quantitatively and comprehensively interrogate a specific time-point in the reaction, and the reaction conditions (start and end points) are precisely known and controlled . The main drawback of a flow tube is that the time-point being studied is generally much shorter than that achieved in a batch reactor, necessitating somewhat higher precursor mixing ratios than are found in the atmosphere. In this study, we model particle growth experiments in a flow tube reactor. The results provide insight into how best to interpret flow tube data and design meaningful experiments. ¶

¶

The focus of this study is particle growth by secondary organic aerosol (SOA) formation.

Moved down [1]: Low and Extremely Low Volatility Organic Compounds (LVOCs and ELVOCs) are able to condensationally grow particles, with LVOCs being limited by the Kelvin effect in small particles (<20 nm). Semivolatile organic compounds (SVOCs) are products with somewhat higher volatility, allowing them to partition between the gas and particle phases

Deleted: .

Deleted: until an equilibrium is established. Oxidized volatile organic compounds (OVOCs) are products which are too volatile to partition to the particles, though they remain available to participate in subsequent gas phase reactions

Moved (insertion) [1]

Deleted: reaction

Deleted: volatile organic compounds (BVOCs)

Deleted: present

Deleted: though

Deleted: ,

Deleted: one or more

and the particle size distribution of aerosol at the exit is measured (Krasnomowitz et al., 2019; Stangl et al., 2019). This setup is well-suited for measuring particle growth rates since the inlet size distribution, outlet size distribution, and time difference between the two are all well known. However, a challenge arises since the growth rate changes as a function of time in the reactor. This time-dependent change is driven by two main processes. First, VOC and oxidant continue to react as aerosol moves through the flow tube, causing the mixing ratios of oxidation products that are able to grow particles to increase with increasing residence time. Fortunately, this effect is readily accounted for if the second order rate constant for the VOC-oxidant reaction is known (Krasnomowitz et al., 2019). Second, the relative rates of the various chemical processes that grow particles can change with increasing precursor mixing ratio and/or particle size (Apsokardu and Johnston, 2018). Accounting for these changes is much more difficult since reaction pathways, rate constants, and physicochemical properties that affect these processes are not fully understood – and lead to uncertainty in predicting ambient levels of SOA (Zhu and Penner, 2019). Because of the complex time dependence of particle growth in a flow tube as well as the impacts of wall loss and condensation sink, simply reporting the growth rate (diameter increase per unit time) based on inlet-outlet size distributions and flow tube residence time is insufficient for predicting growth in other laboratory experiments. The goal of this study is to provide a framework for interpreting flow tube data that gives predictive capability.

Toward this end, we introduce the term "growth factor" (GF) as a way of expressing how SOA formation causes diameter growth of ultrafine particles. GF is defined as the fraction of VOC oxidation products able to enter the particle phase and stay there over the investigated time frame, causing the particle to grow. Defined in this way, GF represents the net uptake of product molecules from the gas phase to the particle referenced to the number of VOC molecules that were oxidized, and its time dependence accounts for the complexities of particle growth in the flow tube. First, we simulate particle growth using a basic SOA formation model that incorporates both surface- and volume- limited growth pathways. We use these simulations to illustrate complex growth kinetics that arise and how they are represented by the time dependence of GF. The simulation also illustrates differences in growth that would be encountered under typical ambient and flow tube conditions, including the sensitivity of GF to precursor gas-phase mixing ratios and the presence of aerosol liquid water (ALW). Finally, we show how GF can be estimated directly from flow tube data (inlet-outlet size distribution, residence time, initial VOC and oxidant mixing ratios). For the SOA simulations described above, we compare the estimated GF to the range of GFs actually inside the flow tube. The estimation method is shown to be a robust way of representing complex growth kinetics from a flow tube experiment, without requiring prior knowledge of the specific chemical processes involved in SOA formation.

2 Simulating Particle Growth by SOA Formation (as Heading 1)

Since we cannot directly measure particle size distributions at various locations inside the flow tube, particle growth must be simulated. The simulation described below contains four key elements: gas-phase kinetics (generation of molecular species capable of growing particles), a range of gas-phase mixing ratios (facilitates comparison of growth kinetics under atmospheric

Moved (insertion) [2]

Deleted: SOA formation in chambers is generally quantified in terms of an aerosol mass yield, defined as the ratio of the mass concentration of organic aerosol produced divided by the mass concentration of VOC consumed, and is interpreted based on the partitioning and condensation of lower volatility products into the organic particle phase . The aerosol mass yield has the potential of being greater than one, since oxidation adds oxygen atoms to the molecule and can give products whose molecular weights are greater than that of the original VOC. Aerosol mass yields for α-pinene ozonolysis have been consistently measured and modelled at approximately 40 % under conditions of high mass concentrations . Aerosol mass yields have been shown to increase 2 to 4 times upon the addition of seed particles, showing a significant dependence on seed size, type, and phase . At low mass concentrations, aerosol mass yields are generally independent of seed particle characteristics, as lower volatile organics will condense while a relatively small fraction of semivolatile organics partition into the particle-phase. As the particle-phase volume increases, the fraction of semivolatile organics that partition into the particle phase increase, simply due to the shift in equilibrium where more particle volume is present to accommodate the additional semivolatile molecules

Moved down [3]: (Apsokardu and Johnston, 2018).

Deleted: While aerosol mass yield is useful for predicting the "end-state" SOA mass concentration, it may be less useful for predicting the kinetics of SOA formation and hence the diameter growth rate of particles. Particle diameter (or particle size distribution) is notably absent from the definition of aerosol mass yield, which only relates total mass/volume of SOA produced to the amount of precursor reacted.¶
¶
In this study, we introduce the term "growth yield" (GY) as a way of expressing how SOA causes diameter growth of particles. GY, defined as the fraction of VOC oxidation events that gives a product able to enter the particle phase and stay there, causing the particle to grow. GY is particle size dependent, since the impact of particle-phase chemistry relative to condensation/partitioning increases in relative importance as the particle size increases

Deleted: Furthermore, GY is likely to be particle composition, phase, and morphology dependent, since these properties determine the types of particle-phase reactions that can occur. Though not explicitly studied here, the Kelvin effect influences condensation/partitioning of small particles (typically <<20 nm diameter) and can also contribute to the size dependence of GY in this size range. As will be described later, GY is a key parameter that can be easily obtained by modelling the growth of particles in a flow tube experiment. In this study, we use an enhanced particle growth model based on our original work (Apsokardu and Johnston, 2018) to explore how GY changes with particle size, composition, and multiphase chemistry. The model is first applied to growth of a single, isolated particle under atmospherically relevant conditions, and then to typical conditions of a flow reactor

Moved up [2]: (Krasnomowitz et al., 2019).

Deleted: The results give insight into how best to set up and interpret flow tube experiments

Deleted: **Modelling procedure**

vs. flow-tube conditions), aerosol growth kinetics (uptake mechanisms of gas-phase molecules on/into the particle), and physicochemical processes and parameters typical of biogenic SOA formation. Gas-phase kinetics in the simulation account for the mixing of VOC and oxidant at the entrance of the flow tube followed by downstream reaction. In principle, aerosol kinetics can take a variety of forms depending on the specific processes involved (Smith et al., 2002; Tolocka et al., 2004b; Zaveri et al., 2018). With respect to particle growth, uptake of gas-phase molecules on/into the particle can be independent of particle diameter, increase with increasing particle diameter, or decrease with increasing particle diameter. Decreasing uptake with increasing particle diameter occurs when uptake is limited by molecular diffusion in the gas-phase, which is relevant only to particles much larger than those considered in this study. Uptake that is independent of particle diameter occurs for surface-limited processes, which includes irreversible condensation of low volatility molecules onto the particle surface and surface-reactions that immobilize (on the timescale of the experiment) semivolatile molecules on the particle surface. Uptake that increases with increasing particle diameter occurs for reactions in the particle phase that immobilize (on the timescale of the experiment) semivolatile molecules within the particle volume.

In order to make these simulations relevant to experimental investigations (Krasnomowitz et al., 2019; Stangl et al., 2019), we use molecular properties and processes typical of α-pinene SOA formation since this system is so well studied over the years (Donahue et al., 2012; Khamaganov and Hites, 2001; Pathak et al., 2007a; Stanier et al., 2007; Trump and Donahue, 2014; Zhang and Zhang, 2005). However, it should be understood that the simulations are not meant to accurately calculate the amount of α-pinene SOA formed. While our simulations include surface- and volume- limited reactions (condensation and oligomerization, respectively) that are fundamental drivers of aerosol kinetics (Smith et al., 2002; Tolocka et al., 2004b), they do not include, for example, reversible dimer formation or the possibility of hindered diffusion within the particle phase – which, depending on conditions chosen, could cause reactions within the particle phase to exhibit either surface- or volume-limited kinetics, or to make volume chemical processes limited by molecular diffusion rather than by the intrinsic rate of reaction (Galeazzo et al., 2021; Zaveri et al., 2020). Hindered diffusion is more complicated to incorporate into the simulations, it is highly specific to the SOA system being studied, and while it would modify the specific growth kinetics in the flow tube, it does not add much to the basic insight gained from the surface- and volume- limited processes already included in the simulations.

The simulation approach used in this study is built upon a foundation previously developed and described elsewhere (Apsokardu and Johnston, 2018). Organic and inorganic species within the simulation include an ammonium sulphate seed particle, organic matter of varying volatility, and water. The relative humidity for all simulations is maintained at a constant 60%, which is between the efflorescence (~35%) and deliquescence (~82%) relative humidities for ammonium sulphate (Gao et al., 2006). The simulation begins with an initial seed particle size that can be set to any diameter and treated as either an effloresced (solid phase) or deliquesced (liquid phase) particle. Organic matter is distributed into six volatility bins which include one non-volatile organic compound (NVOC), four semivolatile organic compounds (SVOCs), and one oxidized

Deleted: The growth model

Deleted: this model

Deleted: Water can be present on the surface of a seed particle (where applicable) and in the gas phase (humidity).

Deleted: humidity points of

Deleted: modelling process

Deleted: at

volatile organic compound (OVOC). Each organic species has the potential to partition/condense between the gas and particle phases based on pre-set volatility parameters, as discussed in Section 2.1. Several particle-phase reactions (dimer formation) are incorporated into the simulation and will be discussed further in Section 2.3. Note that in a real system, e.g., α-pinene SOA formation, a wider range of particle-phase reactions may exist that the set in Section 2.3. Water exists as a predetermined number of monolayers which cover the surface of a solid seed particle when applicable. Previous studies have shown the presence of water on effloresced seed particles under conditions of relative humidity approaching the deliquescence relative humidity point, with thickness of 3 to 5 monolayers for 50 nm particles (Hsiao et al., 2016). By incorporating these various conditions, species, and reactions, we gain insight into the complex growth kinetics occurring inside the flow tube.

2.1 Volatility of organic species (as Heading 2)

Products found in SOA are regularly quantified based on their volatility, which is expressed in terms of saturation concentration (C*) in μg m^{-3}. A study by Donahue et. al. (2012) shows that ambient biogenic emissions contain many species which are highly volatile (C* = 10^6 μg m^{-3}). Although these components are too volatile to partition/condense onto existing particles, oxidation reactions in the atmosphere can produce lower volatility products from these reactants (Chen et al., 2011; Xavier et al., 2019). For the ozonolysis of α-pinene reaction specifically, SOA products have been shown to range in volatility (C*) from < 10^{-1} to > 10^6 μg m^{-3} (Donahue et al., 2012). For this simulation, volatility bins are simplified into three classes as follows: NVOCs, which are non-volatile organics having a C* of 10^{-4} μg m^{-3}, allowing them to condensationally grow particles; SVOCs, which are semi-volatile organics whose volatilities are $10^0 \leq C^* \leq 10^3$ μg m^{-3}; and OVOCs, which are the remaining oxidation products having a C* > 10^3 μg m^{-3} and are too volatile to grow particles in these simulations. The simulations incorporate one type each of NVOC and OVOC, plus four SVOC species, each with a specified volatility. These volatilities are listed in Table 1 alongside their corresponding "product" yields from the ozonolysis reaction. Molar yields of non-volatile ozonolysis products have been measured between 3.5 and 7 % through NO_3. Cl-APi-TOF gas phase measurements in a high volume chamber (Ehn et al., 2014; Sarnela et al., 2018). The product yield (fraction of VOC precursor molecules that react with ozone to give a product molecule in the indicated volatility bin) for NVOC (C* < 10^{-3} μg m^{-3}) is set to 5 % to be consistent with these findings. Product yields for SVOCs and OVOCs are then chosen based on a study by Trump and Donahue (2014), where volatility-based yields ($10^0 \leq C^* \leq 10^3$ μg m^{-3}) were fit to SOA aerosol mass yields utilizing an equilibrium model. As described later, our selection of oxidation products and volatilities in Table 1 allow for a reasonably wide range of volume-limited reaction rates relative to (surface-limited) condensation.

"X" VOC Designation	NVOC	$SVOC_0$	$SVOC_1$	$SVOC_2$	$SVOC_3$	OVOC
Volatility (C*; μg m^{-3})	10^{-4}	10^0	10^1	10^2	10^3	$>10^3$
Molecular Product Yield (%)	5.0	4.0	7.0	9.0	15.0	60.0
Product Mixing Ratios (molecules cm^{-3})	1.0 x 10^7	8.0 x 10^6	1.4 x 10^7	1.8 x 10^7	3.0 x 10^7	1.2 x 10^8

Table 1. Product distribution for VOC ozonolysis used to simulate particle growth.

Deleted: Sect.
Deleted: Multiple
Deleted: this model between
Deleted: partitioned and condensed organic matter
Deleted: Sect.
Deleted: further understanding of
Deleted: effects of SOA on particle
Deleted: ¶
Deleted: model
Deleted: which have
Deleted: and can
Deleted: ,
Deleted: .
Deleted: current model incorporates
Deleted: , one
Deleted: and
Deleted: α-pinene
Deleted: based on
Deleted: derived through
Deleted: ¶
Deleted: 3
Deleted: α-pinene
Deleted: model

2.2 Product mixing ratios (as Heading 2)

For simulating particle growth under atmospherically relevant conditions, constant values for the product mixing ratios are used as shown in Table 1. These values are consistent with what might be observed in a boreal forest during new particle formation (Vestenius et al., 2014). For simulating growth under typical flow tube conditions, product mixing ratios are time dependent and calculated according to Eq. (1):

$$[XVOC]_{g,t+\Delta t} = [XVOC]_{g,t} + k_{II}[VOC]_t[O_3]_t y_{XVOC}\Delta t - k_{WL}[XVOC]_{g,t}\Delta t - k_{CS}[XVOC]_{g,t}\Delta t \quad (1)$$

where $[XVOC]_{g,t}$, $[VOC]_t$, and $[O_3]_t$ are the respective mixing ratios at time t, Δt is the time increment, and y is the molar yield of the respective XVOC ozonolysis product. Here, three processes are represented; the oxidation of VOC by ozone based on a second order rate constant (k_{II}), the loss of products to the inner walls of the flow tube (k_{WL}), and loss of products to the condensation sink (k_{CS}). The [XVOC] designation represents each of the six species in Table 1: NVOC, $SVOC_{0\text{-}3}$, and OVOC, i.e., a separate equation for each volatility product.

2.3 Simulating particle growth (as Heading 2)

The amount of seed particle growth obtained for a given simulation is evaluated with respect to condensation, partitioning and reaction of organic species. Partitioning and reaction of SVOC occur in the portion of the particle considered to be liquid-like. For the purposes of this study, the liquid-like fraction of the particle volume is simply taken as the total amount of organic and aqueous volume in the particle at any time point in the simulation. Calculations are performed recursively, updating gas- and particle-phase concentrations every tenth of a second over the timescale of the simulation. Particle-phase concentrations for each species are calculated according to Eqs. (2-4) at each timepoint based on the gas-phase product yields discussed previously.

$$[NVOC]_{P,t+\Delta t} = [NVOC]_{P,t} + \frac{c}{2}\gamma[NVOC]_{g,t}\frac{S_P}{V_P}\Delta t - k_D[NVOC]_{P,t}[SVOC]_{P,t}\Delta t \quad (2)$$

$$[SVOC]_{P,t+\Delta t} = [SVOC]_{P,t} + \frac{c}{2}\gamma[SVOC]_{g,t}\frac{S_P}{V_P}\Delta t - k_D[NVOC]_{P,t}[SVOC]_{P,t}\Delta t \quad (3)$$

$$[DIMER]_{P,t+\Delta t} = [DIMER]_{P,t} + k_D[NVOC]_{P,t}[SVOC]_{P,t}\Delta t \quad (4)$$

Here, $[XVOC]_{P,t}$ and $[DIMER]_{P,t}$ are the respective particle-phase concentrations at time t, $[XVOC]_{g,t}$ and $[DIMER]_{g,t}$ are the respective gas-phase concentrations at time t, c is the mean thermal velocity, γ is the uptake coefficient (C* dependent), S_p is the surface area of the particle, V_p is the volume of the particle, Δt is the time increment, and k_D is the second order rate constant for dimer formation. Dimerization rate constants have been reported on the order of 10^{-4} to 10^{-2} $M^{-1}s^{-1}$ for various reactions of hydroperoxides and aldehydes (Ziemann and Atkinson, 2012). Of the many products formed during SOA formation, approximately 50 % of the mass formed from α-pinene has been reported to have a peroxide functionality (Docherty et al., 2005). Accordingly, a rate constant of 10^{-2} $M^{-1}s^{-1}$ is used for all simulations. The saturation ratio (S_d) determines how well a gas-phase compound partitions into the particle phase and is defined as the ratio of gas-phase mixing ratio to the saturation

Deleted: ¶
Deleted: modelling single
Deleted: modelling
Deleted: $[\alpha P]_t$
Deleted: αP
Deleted: VOC for α-pinene
Deleted: α-pinene
Deleted: $SVOC_i$
Deleted: .
Deleted: product
Deleted: . The development and application of this equation for flow tube modelling has been described elsewhere in detail .
Deleted: Modelling
Deleted: the
Deleted: /condensation
Deleted: onto
Deleted: and/or into
Deleted: phase (where applicable). Modelling
Deleted: reclusively
Deleted: /[
Deleted: /[
Deleted: molecular
Deleted: The
Deleted: in this study is held at 10^{-2} $M^{-1}s^{-1}$

mixing ratio. A high ratio (S_d >> 1) is found in species that condensationally grow particles, such as NVOCs. As SVOCs partition between the gas and particle phase, they grow particles at a slower rate due to a S_d << 1. It is important to note that Eq. (3) is written for this situation. However, if and when $S_d \geq 1$ for SVOC, no additional flow into the particle phase would occur unless the formation of DIMER shifted the equilibrium by depleting the particle-phase concentration. Particle-phase reactions responsible for dimer formation are simplified and represented by the term $k_D[NVOC]_{P,t}[SVOC]_{P,t}\Delta t$ in these equations. In principle, this term represents all possible combinations of NVOC and $SVOC_i$ molecules to form a DIMER. However, the simulations shown in this study include just one specific DIMER formation reaction – two $SVOC_0$ molecules reacting with each other. Simulations including the full range of DIMER formation reactions have been performed, but they add very little to calculated diameter growth (most of the growth is due to $SVOC_0$ only) or to the time dependence of GF in the flow tube. Therefore, in the interest of simplicity for discussion of this work, only the $SVOC_0$ dimerization simulations are shown. Each organic molecule and/or compound with a low enough volatility to remain in the particle phase is summed at each timepoint, representing any increase in particle volume (V_P) over the previous timepoint. This is represented by Eq. (5):

$$V_{P,t+\Delta t} = V_{P,t} + [NVOC]_P V_{NVOC}\Delta t + [SVOC]_P V_{SVOC}\Delta t + [DIMER]_P V_{DIMER}\Delta t \quad (5)$$

where V_{NVOC}, V_{SVOC}, and V_{DIMER} are the respective molecular volumes contributing to particle growth. Diameter growth of the particle is determined by Eq. (6):

$$d_{t+\Delta t} = 2\left(\sqrt[3]{\frac{3(V_{P,t+\Delta t})}{4\pi}}\right) \quad (6)$$

2.4 Growth factor (as Heading 3)

Growth factor (GF) is defined as the fraction of all oxidation products colliding with the particle surface that are actually taken up into the particle causing it to grow, as defined by Eq. (7):

$$GF_t = \left(\frac{NVOC+SVOC_i+OVOC\ taken\ up\ into\ the\ particle}{NVOC+SVOC_i+OVOC\ striking\ the\ particle\ surface}\right)_t \quad (7)$$

GF is calculated for each time increment based on the amount of growth caused by each oxidation product during that increment. In practice, GF includes the full NVOC yield (except for particles << 20 nm, where the Kelvin effect causes some NVOC molecules to remain in the gas phase) plus a portion of the $SVOC_i$ yield depending upon how significant partitioning is and how much of the partitioned $SVOC_i$ undergoes reaction in the particle phase to produce a non-volatile DIMER. In this study, OVOC does not contribute to GF since its concentration in the particle phase is too small to efficiently form DIMER.

Deleted: in terms of

Deleted: case, which is applicable for all simulations in this study

Deleted: However, this term includes any combination of NVOCs and SVOCs able to form a DIMER in each volatility bin.

Deleted: -phase

Deleted: attributing

Deleted: For effloresced seeded simulations, the initial V_P is equal to zero as the seed is considered to have a solid core, increasing as organic matter condenses and forms an organic layer. In the case of water monolayers being added to the same seed particle, this value is equivalent to the volume of water on the surface of the particle. For deliquesced seed particles, V_p is equal to the entire initial volume of the particle at the beginning of the simulation.

Deleted: is

Deleted: as shown

Deleted: yield

Deleted: yield (GY

Deleted: $GY_t = \left(\frac{NVOC+SVOC_i+OVOC\ taken\ up\ into\ the\ particle OC\ uptake\ collisions}{NVOC+SVOC_i+OVOC\ striking\ the\ particle\ surface Total\ surface\ collisions}\right)_t$ (7)¶ GY

Deleted: GY

Deleted: GY

3 Particle growth under atmospherically relevant conditions (as Heading 1)

The first simulations examine the effects of condensation of NVOC, partitioning of SVOC, and DIMER formation on particle growth under atmospherically relevant, low-growth (<1 nm/hr) conditions, as a base case for comparison to flow tube simulations. Calculations in this section utilize the product mixing ratios listed in Table 1 and are held constant throughout the growth of the particle. Figure 1a shows 5 nm dia. dry (no aerosol liquid water, ALW) ammonium sulphate seed particles growing to 100 nm by condensation of NVOC and partitioning of SVOC alone. Here, GF remains constant at 5% throughout the simulation as NVOC condensationally grows the particle. Although SVOC partitions between the gas and particle phase, the steady state amount in the particle phase is too low to have a significant contribution to particle growth. Figure 1b shows the same simulation but with the addition of DIMER formation. Recall that for the simulations shown, DIMER formation is restricted to between two SVOC molecules with a C* equal to 10^0 μg m^{-3}. Note that GF starts at 5 % as in Figure 1a. Since SVOC partitioning requires an organic phase (no ALW in this simulation), NVOC must build up on the particle surface in order to provide a medium for SVOC partitioning and subsequent DIMER formation. Relative to condensation/partitioning alone in Fig. 1a, DIMER formation increases the rate of particle growth in Fig. 1b (note the slightly shorter time scale to reach 100 nm) and results in an increase of GF with increasing particle size.

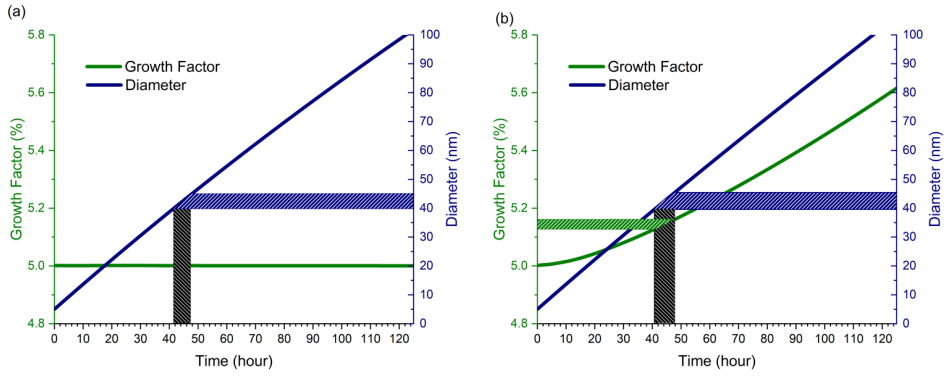

Figure 1: Growth factor and diameter vs. time for dry (no ALW) ammonium sulphate seed particles with an initial diameter of 5 nm. (a) Condensation of NVOCs and partitioning of SVOCs only. (b) $SVOC_0$ DIMER formation in addition to condensation and partitioning.

Also shown in the Figure 1 plots are shaded regions depicting what a flow tube experiment might look where a relatively small time-slice of the overall growth process is studied, in this case highlighting a time period where 40 nm dia. particles grow to 45 nm. Particle growth during this time period is associated with a specific GF that changes depending upon whether or not

Deleted: Single

Deleted: 3.1 Particle growth with and without particle-phase chemistry (as Heading 3)¶

Deleted: series of calculations examines…imulations examine the effects of condensation of NVOC, partitioning of SVOC, and oligomerization reactions ... [1]

Deleted: , which serves

Deleted: All simulations

Deleted: a … nm effloresced…ia. dry (no aerosol liquid water, ALW) ammonium sulphate seed particle grown ... [2]

Deleted: GY…F remains constant at 5 ... [3]

Deleted: While…lthough SVOC partitions between the gas and particle phase, it ... [4]

Deleted: volatile…ow to have any ... [5]

Deleted: plus the potential …ut with the addition of DIMER formation. Recall that for DIMER formation. Throughout this study…he simulations shown, DIMER formation is noted as D.SV_0, where a DIMER can only be formed ... [6]

Deleted: in the particle phase

Deleted: the GY curve…F starts at 5 %, the same as if condensation were the only process attributing to growth yiel ... [7]

Deleted: a particle phase, the absence of SVOCs lead to no immediate effect on particle growth due to particle-phase chemistry. However, once approximately one monolayer of NVOCs buil ... [8]

Deleted: follows quickly afterwards. This speeds up

Deleted: in GY

Deleted: rate (GR) is a measure of how quickly a particle grows. Since this term is determined by the size of the entire particle, it is subject to particle losses to the reactor walls and condensation ... [9]

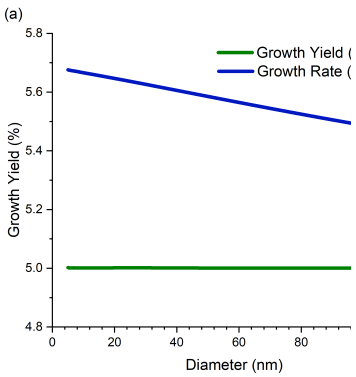

Deleted: ... [10]

DIMER formation occurs. If only condensational growth occurs i.e., surface-limited kinetics (Figure 1a), then the aerosol growth kinetics over this time period are straight forward – GF remains constant at 5.0%. If both surface- and volume-limited kinetics occur (Figure 1b), then the aerosol growth kinetics become more complex since GF increases slightly over the shaded time period. While the change in aerosol growth kinetics is small in Figure 1b, the next section shows that such changes are greatly amplified under conditions typically used flow tube experiments.

4 Particle growth inside a flow tube reactor (as Heading 1)

In this and subsequent sections, particle growth is simulated under conditions typically used in our flow tube reactor, whose design and performance are described in detail elsewhere (Krasnomowitz et al., 2019). In our laboratory experiments, size selected ammonium sulphate seed particles are introduced into the flow tube along with gas-phase VOC (α-pinene in our initial experiments), ozone, cyclohexane (hydroxyl radical scavenger), and water vapor (relative humidity control). Particle residence time in the flow tube is approximately 4 min, much shorter than the shaded region in Figure 1. Experimental conditions must be chosen such that particles exiting the flow tube reactor have increased from their initial diameters by about 1 to 8 nm, which is sufficient for high precision measurement using a Scanning Mobility Particle Sizer (TSI, Inc., Shoreview, MN). This range of diameter increase corresponds to a growth rate between about 15 and 120 nm hr^{-1}. For comparison, ambient particle growth rates are on the order of 1 to 10 nm hr^{-1} for new particle formation events. To achieve the desired amount of particle growth, we typically perform flow tube experiments with a VOC mixing ratio on the order of 10 ppbv and ozone mixing ratios between 30 to 300 ppbv (Krasnomowitz et al., 2019). Similar parameters have been used by others (Pathak et al., 2007b) to experimentally study SOA formation by α-pinene ozonolysis.

4.1 Particle growth inside a flow tube with and without particle-phase chemistry (as Heading 3)

The first set of flow tube simulations start with 40 nm dia. dry (no ALW) ammonium sulphate seed particles that are mixed with VOC (11 ppbv) and ozone (200 ppbv) at the inlet to the flow tube. As aerosol travels through the flow tube (4 min residence time), VOC and ozone react causing the seed particles to grow. NVOC and SVOC gas-phase mixing ratios increase with increasing time as calculated by Eq. (1) using the molecular product yields in Table 1. DIMER formation is calculated from all relevant reactant combinations as described in Section 2.3. Figure 2 shows the change in particle diameter and GF with time for simulations analogous to those in Figure 1. Fig. 2a simulates growth by condensation of NVOC and partitioning of SVOC. Fig. 2b simulates growth by condensation, partitioning, and DIMER formation.

Moved down [4]: Fig.

Moved down [5]: Fig.

Deleted: 3 involve the condensation of NVOCs, partitioni ... [11]

Deleted: 1 for the respective seed phase. As discussed pre ... [12]

Deleted: **in**

Deleted: section

Deleted: modelled

Deleted: Briefly

Deleted: (solid or liquid-like; 40, 60, or 80 nm dia.)

Deleted: in

Deleted: BVOC

Deleted: four minutes.

Deleted: are

Deleted: can be measured with

Deleted: .).

Deleted: (and the simulations in the previous section, whi ... [13]

Deleted: an α-pinene

Deleted: 11

Moved down [6]: Fig.

Deleted: . Similar parameters have been used by others a ... [14]

Deleted: 4d. Here, the same conditions for condensation, ... [15]

Deleted: Figure 6 shows the growth yields as a function o ... [16]

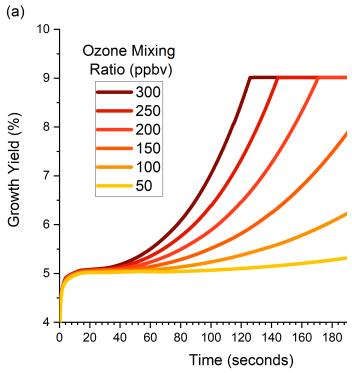

Deleted: ... [17]

Deleted: **for a single**

Moved (insertion) [4]

Moved (insertion) [5]

In Fig. 2a, GF remains constant at 5% throughout the timescale of the simulation. As for the simulation in Fig. 1a, particle growth in Fig. 2a is driven by condensation of NVOC. Even though the particle growth rate is different for the two simulations, GF is the same since the molar yield of NVOC is the same, even though the simulation conditions are quite different. These figures illustrate the relative simplicity of surface-limited growth kinetics in a flow tube. In contrast, the GF plot in Fig. 2b is time dependent and differs substantially in shape and numerical value from Fig. 1b. GF for Figs. 2a and 2b both start at 5% because only NVOC condensation contributes to growth in the absence of a reactive particle phase. However, once an organic coating forms on top of the particle surface, $SVOC_0$ partitioning and DIMER formation begin to occur within this coating. GF increases above 5% because some $SVOC_0$ molecules striking the particle surface react to form DIMER, causing a net flow of $SVOC_0$ from the gas phase to the particle. Since DIMER formation follows volume-limited kinetics, the rate of $SVOC_0$ uptake increases as the organic volume on the particle increases, and therefore GF increases as well. Eventually, the organic volume becomes large enough that the rate of $SVOC_0$ uptake reaches a maximum, given by mass flux from the gas phase to the particle surface. At this point, particle growth changes from volume-limited to surface-limited kinetics, and GF becomes approximately independent of time. The magnitude of GF at the end of the simulation is given by the combined molecular product yields of NVOC and $SVOC_0$ (5% + 4% = 9%) plus a small amount of growth due to partitioning of other SVOCs, giving a total GY of ~9.1-9.2%. GF in Fig. 2b rises much faster and to a higher numerical value than Fig. 1b because DIMER formation is nonlinear with respect to $SVOC_0$ gas-phase mixing ratio (Apsokardu and Johnston, 2018). The difference between Figs. 1b and 2b illustrate the complexity of particle growth on starting conditions when volume-limited kinetics apply, and how volume-limited reactions can give surface-limited growth kinetics in the high precursor mixing ratio environment of a flow tube.

Moved (insertion) [3]

Deleted: particle: (a) effloresced

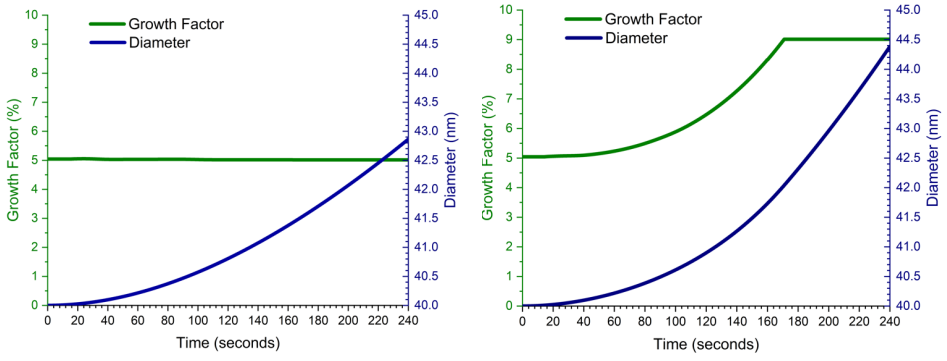

Figure 2: Growth factor and particle diameter vs. time for 40 nm dia. ammonium sulphate seed particles traveling through the flow tube, growing by (a) condensation of NVOC and partitioning of SVOC alone, and (b) with $SVOC_0$ DIMER formation included.

4.2 Particle growth inside a flow tube as a function of ozone mixing ratio (as Heading 3)

This subsection explores the high mixing ratio environment of a flow tube in more detail. Simulations in this section have an expanded range of ozone mixing ratios between 50 and 300 ppbv, which are typical for our flow tube experiments (Krasnomowitz et al., 2019). Figure 3 shows GF vs. time for six different ozone mixing ratios. (For reference, the 200 ppbv plot in Fig. 2b is replotted in Fig. 3.) The nonlinear dependence of GF on ozone mixing ratio is readily apparent in this plot. For the lowest mixing ratio, GF hardly increases at all as growth is driven mostly by NVOC condensation. As the ozone mixing ratio increases, GY also increases and as discussed in the previous subsection, eventually reaches the maximum value possible when growth due to DIMER formation becomes surface-limited. The higher the ozone mixing ratio, the faster that surface-limited kinetics are reached. While the growth kinetics are complex, Figure 3 illustrates how the mixing ratio dependence can be used to determine whether nonlinear and/or volume-limited processes contribute to the growth kinetics. It also gives caution that one should fully consider these types of processes when extrapolating flow tube experiments back to ambient conditions.

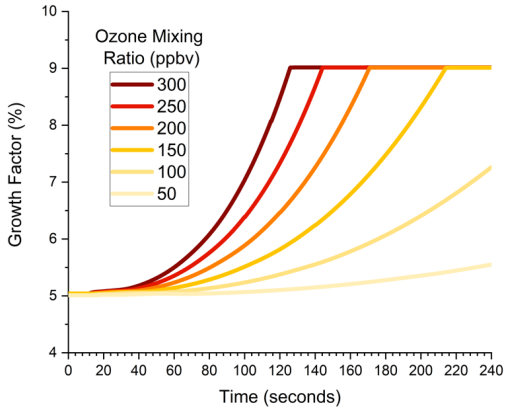

Figure 3: Growth factor vs. time in the flow tube for 40 nm ammonium sulphate seed particles. Condensation, partitioning, and DIMER formation are all included. Ozone mixing ratio is shown with increasing colour intensity corresponding to increasing mixing ratio.

Moved (insertion) [7]

Deleted: deliquesced

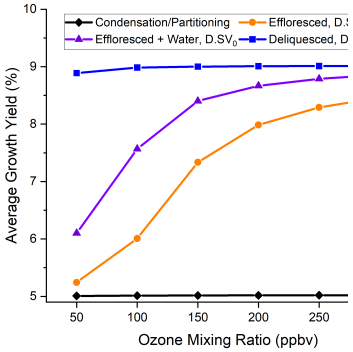

Deleted:
Figure 7: Average growth yield vs. ozone mixing ratio for the 40 nm dia. ammonium sulphate seed particles and conditions shown in Figures 4 and 5. Lines are drawn as an aid to the eye. ¶

¶

While the ability of particle-phase chemistry to increase GY generally increases with increasing particle diameter, Fig. 5 shows that this effect can be muted if the reaction is very fast and growth becomes surface- rather than volume-limited over a significant portion of the flow tube. In these situations, decreasing the ozone mixing ratio can enhance the particle size dependence by lowering the reaction rate and moving away from surface-limited kinetics. This is illustrated in Fig. 8 for deliquesced particles from 40 to 80 nm, which represents a "worst-case" situation for the various simulations studied. When the ozone mixing ratio is high, the GY for all three particle sizes converges toward the maximum value (9 %). When the mixing ratio is lowered, the GY for the three sizes begin to diverge because volume-limited kinetics encompass a greater portion of time in the flow tube. Even when the diameter dependence of the GY in a flow tube obscures volume-limited kinetics (Fig. 5), the existence of particle phase chemistry can be inferred from the GY dependence on seed particle composition and/or phase e.g. average GY of deliquesced vs. effloresced particles in Fig. 5.¶ ... [18]

4.3 Impact of aerosol liquid water (ALW) on particle growth (as Heading 3)

This subsection explores how ALW, either on the particle surface or within the particle volume can enhance growth. In these simulations, the presence of ALW simply increases the volume in which particle-phase chemistry can occur. In other words, SVOC partitioning and DIMER formation are assumed to be independent of whether the reactive phase is aqueous, organic, or a combination of the two. Of course, in experimental systems this probably is not the case, but the purpose of these simulations is to explore the effect of total reactive volume, not phase-dependent chemistry. Up to now, all simulations have involved "dry" ammonium sulphate particles, meaning the particles were effloresced without any water molecules on the surface. However, Hsiao et al., 2016 showed that approximately 3 to 5 monolayers of water molecules can exist on the surface of an effloresced ammonium sulphate particle with a relative humidity near but below the deliquescence point. Note that a coverage of 5 monolayers corresponds to an aqueous layer thickness of almost 2 nm based on a density of 1.00 g mL^{-1} and a molecular diameter of 0.385 nm. In principle, surface water could provide sufficient volume at the beginning of a growth experiment for SVOC partitioning and DIMER formation to occur. If the relative humidity is high enough for the particle to deliquesce, then the entire volume would be available for SVOC partitioning and DIMER formation, and a large enhancement of SVOC partitioning and DIMER formation would be expected. These possibilities are examined in Figure 4.

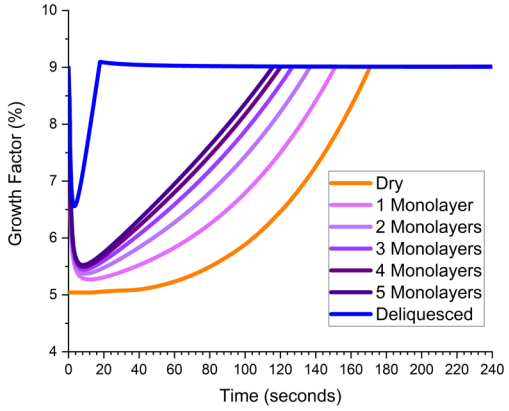

Figure 4: Growth factor vs. time in the flow tube for dry (no ALW) ammonium sulphate seed particles (orange), effloresced seed particles initially containing 1-5 water monolayers on the surface (purple shades), and deliquesced seed particles (blue). Condensation, partitioning, and DIMER formation are all included. The ozone mixing ratio is 200 ppbv.

Deleted: interfacial

Deleted: As shown in Fig. 7, the addition of water monolayers on the surface of an effloresced seed particle enhances DIMER formation significantly. An in-depth examination of this effect is shown in Fig. 9, where the growth due to condensation, partitioning, and particle-phase reactions of 40 nm seed particles of varying phase and surface water content are simulated. Here, effloresced seed particles take the longest amount of time to reach complete uptake of NVOCs and SVOCs for particle growth. Monolayers of water ranging from one to five layers thick are added to the same particle, significantly increasing the uptake of SVOCs over that of the effloresced seeded simulation. The simulation of a deliquesced seed particle is included for comparison to a particle of the same size where the entire volume is considered to be the particle phase. The plots in Figs. 5, 7, and 9 illustrate the relatively large impact of surface water on DIMER formation and highlight the importance of fully characterizing the air-particle interface in both laboratory and field settings. ¶

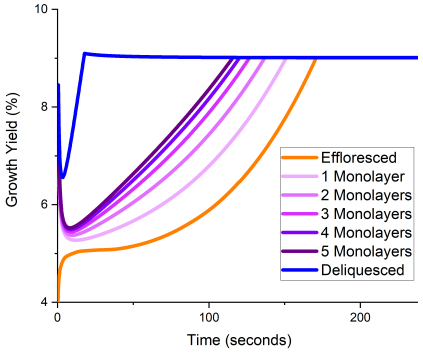

Figure 9

Deleted: yield

Deleted: an effloresced

Deleted: particle

Deleted: an

Deleted: particle

Deleted: for a

Deleted: particle

The "dry" particle simulation in Figure 4 is the same as that in Fig. 2b. GF is 5% at the beginning of the simulation and increases with increasing time, slowly at first because NVOC condensation is needed to grow the organic layer where DIMER formation can occur. When surface water is available at the outset, a significant volume for DIMER formation already exists. Fig. 4 shows that even a single monolayer is able to enhance GF, and the enhancement increases as the number monolayers increases. GF is highest for deliquesced particles where the full particle volume is available for partitioning and reaction. The time dependence of GF for particles containing ALW contains a feature not observed in previous simulations. Initially, GF is very high and then drops with increasing time. The initial spike in GF is associated with SVOC uptake into the aqueous volume to establish the partitioning equilibrium. Once equilibrium is established, GF drops but then later starts to increase again as DIMER formation becomes significant. GF reaches its maximum value in all simulations, but the time point that the maximum is achieved decreases as the amount of ALW increases. Figure 4 shows that surface water has the capability to dramatically increase particle growth by processes that are volume-limited. It also gives caution that contaminants on the particle surface may substantially alter growth kinetics if they are uncontrolled and influence the initial volume available for reaction.

Moved (insertion) [6]

Deleted: included

5 Interpreting Flow Tube Measurements (as Heading 1)

As discussed in Section 1, flow tube reactors are well-suited for measuring particle growth rates (and comparing growth under different experimental conditions) since the inlet size distribution, outlet size distribution, and time difference between the two are all determined. However, the simulations in Section 4 show that growth kinetics inside the reactor are complex and not easily predicted unless one already understands the growth processes in detail. Given this complexity, how does one extract useful growth information from an experiment when the processes leading to growth are poorly understood? In this section, we discuss a method to use flow tube data to determine GF without knowledge of the growth processes involved. For the simulations in Section 4, we compare GFs obtained from this interpretive method to the actual GFs from the simulations.

The interpretive method is based on five measured quantities and one known kinetic parameter: gas-phase VOC mixing ratio at the inlet, gas-phase oxidant mixing ratio at the inlet, particle size at the inlet, particle size at the exit, residence time of the reactor, and the second order rate constant for reaction of VOC and oxidant. From these measurables and parameters, GF is calculated for condensed organic vapor (COV), which is defined as the group of oxidation products that grew particles in a given time period. In the context of the simulations in Section 4, COV includes all non-volatile products (NVOC) that irreversibly condense onto the particle plus the portion of semi-volatile products (SVOC) that partition into the particle phase, react, and stay there on the time scale of the full simulation. In the simulations, SVOC uptake is calculated, and from it, particle growth (change in diameter) and GF are determined. The interpretive method takes the opposite approach. The "measured" change in particle diameter from inlet to outlet is used to back calculate what GF had to be in order to produce this change. With the interpretive method, diameter growth of particles between inlet and outlet are determined by integrating Eq. 8 and 9 over the residence time of the reactor:

Deleted: In the simulations so far, the diameter growth of particles and corresponding GY were calculated as a function of time using a specific chemical model of the growth processes. In a flow tube experiment where growth is compared for various gas- and particle-phase conditions, the opposite occurs. Diameter growth is measured at the outlet of the flow tube, which corresponds to a single time-point in the process, and from that an average GY is determined and interpreted in the context of various chemical growth models. Because no specific model is assumed, the various oxidation products represented by Eq. (1) are replaced by a single growth species:¶

$$[COV]_{g,t+\Delta t} = [COV]_{g,t} + k_{II}[\alpha P]_t[O_3]_t y_{COV}\Delta t - k_{WL}[COV]_{g,t}\Delta t - k_{CS}[COV]_{g,t}\Delta t \rightarrow\rightarrow \quad (8)$$¶

where y_{COV} is the yield of condensable organic vapor (COV) that is able to grow the particles. The modelling process fits the lone adjustable parameter (y_{COV}, which is also defined as the growth yield, GY) so that the calculated diameter change at the exit of the flow tube matches the measured value. More details on modelling experimental data can be found elsewhere

$$\frac{d(d_P)}{dt} = \frac{c}{2}\gamma[\mathrm{COV}]_t\beta_d V_{\mathrm{COV}} \quad (8)$$

where: c is mean thermal velocity, γ is the uptake coefficient (assumed to be 1 in this work), $[\mathrm{COV}]_t$ is the time-dependent gas-phase COV mixing ratio, β_d is the correction factor for mass flux to a spherical particle with diameter d, and V_{COV} is the molecular COV volume. When calculating the diameter change, all COV molecules are assumed to have an average molecular weight of 200 g/mol and an average density of 1.2 g/cm^3, which are typical for biogenic VOC oxidation products. The processes which supply COV to and deplete COV from the system are accounted for in an analogous way to Eq. 1:

$$\frac{d[COV]_t}{dt} = (k_{II}[VOC]_g[O_3]_g)(GF) - k_{WL}[COV]_t - k_{CS}[COV]_t \quad (9)$$

In Eq. 8 and 9, the only unknown parameter is GF, which is adjusted to make the calculated outlet minus inlet diameter change match the measured change. Importantly, the interpretive method is based only on experimental observables, and no assumptions are made about the actual growth processes used for simulating SOA formation. An important point to note is that the wall loss and condensation sink terms in Eq. 9 are what make it difficult to simply compare outlet minus inlet particle diameter changes from one flow tube experiment to the next, since the magnitudes of these terms affect how much growth is observed and they are not necessarily constant from experiment to experiment. Growth factor overcomes this problem and is specific to the VOC system being studied.

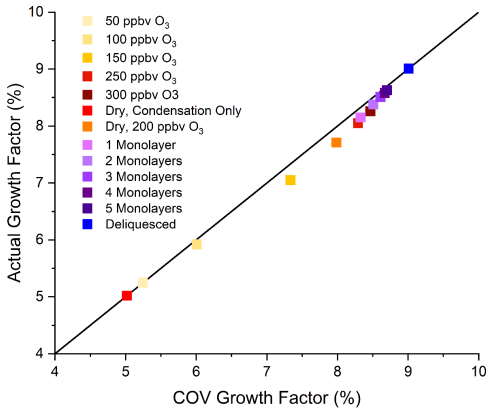

Figure 5: COV Growth Factor obtained from outlet minus inlet diameter change vs. Actual Growth Factor (average of GFs within the flow tube for each simulation in Section 4). Colours correspond to those shown for the simulations in Figures 3 and 4. The line shows a 1:1 ratio.

Figure 5 shows how well the COV growth factors determined from the interpretive method ("empirical" GF from Eq. 8 and 9) match the average of the simulated GFs ("actual") inside the flow tube from Section 4. For comparison, a 1:1 line is also shown. Overall, the two sets of GFs deviate only slightly from each other, and the deviation is much less than the uncertainty encountered in our experimental measurements, which is typically on the order of +/- 10% or less of the reported COV growth factor. Figure 5 gives confidence that the empirical GFs obtained from the interpretive method give a close approximation of the actual GFs inside the flow tube.

It is important to realize that the simulations in Section 4 and the COV calculation in Section 5 are not simply "reverse" calculations of each other. The simulations in Section 4, though simplified relative to detailed SOA formation models for specific VOC precursors, incorporate numerous chemical details including relative yields and volatilities of VOC oxidation products (NVOC, SVOC, OVOC), DIMER reaction partners, volatilities of the reaction partners, second-order rate constant for DIMER formation, and the portion of the particle volume capable of supporting DIMER formation. *None* of these details are included in the COV calculations, which simply determine how many gas phase molecules (i.e., the fraction of VOC oxidation products) that had to go onto/into the particle to cause the outlet minus inlet diameter change for each simulation. The GFs obtained from COV calculations accurately represent the actual GFs, and as such should allow the prediction of particle growth in new experiments without detailed foreknowledge of growth mechanisms.

6 Conclusions (as Heading 1)

Flow tubes provide an effective way to study particle growth as a function of seed particle size, composition, and phase state, as well as other conditions such as precursor mixing ratios and relative humidity. Although these experiments provide a simple measure of size distribution change over a defined length of time, the growth mechanisms that contribute to particle growth can be complex and vary in terms of oxidized product volatilities, yields, and reaction rates. This study highlights how particle phase chemistry can change aerosol kinetics within the flow tube when compared to growth by NVOC condensation alone. The presence of aerosol liquid water is shown to be capable of enhancing particle growth by increasing the amount of volume available for reaction. Even one or a few monolayers of water on the surface of an effloresced particle can significantly enhance growth by providing a medium for particle phase chemistry to occur. Since the specific reactions driving aerosol growth kinetics are often unknown or only partially understood for many SOA systems, an empirical calculation of COV growth factor based on outlet minus inlet particle diameters in a flow tube experiment can give predictive capability for SOA growth. In the present study, empirical COV growth factors closely matched the actual GFs from SOA simulations, and one can expect that the difference between empirical and actual growth factors in flow tube experiments will be within typical experimental uncertainties.

Moved up [7]: (Krasnomowitz et al., 2019).

Deleted: Similar to the model in Sect. 2, COV in Eq. (8) encompasses all NVOC plus a portion of SVOC that is able to enter the particle and stay there. Unlike the model in Sect. 2, y_{COV} is assumed to be constant across the length of the flow tube since only a single growth species is assumed. The first question to ask is how well the GY calculated from the approach in Eq. (8) matches the average GY in Figs. 5, 7 and 8. To answer this question, we used the modelling approach of Sect. 2 to determine the diameter change at the time-point particles would exit the flow tube, and then we determined the COV by the approach in Eq. (8). Figure 10 compares the average GY to the COV yield for 40, 60, and 80 nm seed particles under the condition of 200 ppbv ozone. When DIMER formation is excluded from the simulation, both the average GY and COV yield give the same value – 5 % which corresponds to the NVOC yield. When DIMER formation is included in the simulation and the conditions are such that surface-limited kinetics exist throughout the flow tube, both the average GY and COV yield give the same value: 9 % which corresponds to the sum of NVOC and SVOC yields. In between these two extremes where volume-limited kinetics exist in at least part of the flow tube, the average GY and COV yield track each other closely and deviate at most by at most a few percent of the respective values. At a yield of 5 %, all values are equivalent as the same condensational growth process is being modelled in both methods.¶ ... [19]

Deleted: This modelling study shows that through a combination of seed particle size and precursor mixing ratio dependencies, insight can be gained into kinetic limitations (volume- vs. surface-limited growth). These dependencies, in combination with other var ... [20]

Deleted: additional constraints on

Deleted: types of chemical processes responsible

Deleted: growth. Finally,

Deleted: simulations show the disproportionate ability of

Deleted: surface to

Deleted: -

Deleted: , highlighting

Deleted: need to characterize

Deleted: air-particle interface.

Author Contribution

MT and DH performed the simulations and COV calculations. MT prepared the manuscript with contributions from all authors.

Deleted: for modelling particle growth

Competing Interests

The authors declare that they have no conflict of interest.

Acknowledgements

This research was supported by two grants from the U.S. National Science Foundation, CHE-1904765 and AGS-1916819.

References

Apsokardu, M. J. and Johnston, M. V.: Nanoparticle growth by particle-phase chemistry, Atmos. Chem. Phys., 18(3), 1895–1907, doi:10.5194/acp-18-1895-2018, 2018.

Barsanti, K. C. and Pankow, J. F.: Thermodynamics of the formation of atmospheric organic particulate matter by accretion reactions-Part 3: Carboxylic and dicarboxylic acids, Atmos. Environ., 40(34), 6676–6686, doi:10.1016/j.atmosenv.2006.03.013, 2006.

Bell, M., Davis, D. L. and Fletcher, T.: A retrospective assessment of mortality from the London smog episode of 1952: The role of influenza and pollution, Environ. Health Perspect., 112(1), 6–8, doi:10.1289/ehp.6539, 2004.

Bianchi, F., Kurtén, T., Riva, M., Mohr, C., Rissanen, M. P., Roldin, P., Berndt, T., Crounse, J. D., Wennberg, P. O., Mentel, T. F., Wildt, J., Junninen, H., Jokinen, T., Kulmala, M., Worsnop, D. R., Thornton, J. A., Donahue, N., Kjaergaard, H. G. and Ehn, M.: Highly Oxygenated Organic Molecules (HOM) from Gas-Phase Autoxidation Involving Peroxy Radicals: A Key Contributor to Atmospheric Aerosol, Chem. Rev., 119(6), 3472–3509, doi:10.1021/acs.chemrev.8b00395, 2019.

Chen, Q., Liu, Y., Donahue, N. M., Shilling, J. E. and Martin, S. T.: Particle-phase chemistry of secondary organic material: Modeled compared to measured O:C and H:C Elemental ratios provide constraints, Environ. Sci. Technol., 45(11), 4763–4770, doi:10.1021/es104398s, 2011.

Crounse, J. D., Nielsen, L. B., Jørgensen, S., Kjaergaard, H. G. and Wennberg, P. O.: Autoxidation of organic compounds in the atmosphere, J. Phys. Chem. Lett., 4(20), 3513–3520, doi:10.1021/jz4019207, 2013.

Després, V. R., Alex Huffman, J., Burrows, S. M., Hoose, C., Safatov, A. S., Buryak, G., Fröhlich-Nowoisky, J., Elbert, W., Andreae, M. O., Pöschl, U. and Jaenicke, R.: Primary biological aerosol particles in the atmosphere: A review, Tellus, Ser. B Chem. Phys. Meteorol., 64(1), 1–58, doi:10.3402/tellusb.v64i0.15598, 2012.

Docherty, K. S., Wu, W., Lim, Y. Bin and Ziemann, P. J.: Contributions of organic peroxides to secondary aerosol formed from reactions of monoterpenes with O3, Environ. Sci. Technol., 39(11), 4049–4059, doi:10.1021/es050228s, 2005.

Donahue, N. M., Kroll, J. H., Pandis, S. N. and Robinson, A. L.: A two-dimensional volatility basis set-Part 2: Diagnostics of organic-aerosol evolution, Atmos. Chem. Phys., 12(2), 615–634, doi:10.5194/acp-12-615-2012, 2012.

Ehn, M., Thornton, J. A., Kleist, E., Sipilä, M., Junninen, H., Pullinen, I., Springer, M., Rubach, F., Tillmann, R., Lee, B., Lopez-Hilfiker, F., Andres, S., Acir, I. H., Rissanen, M., Jokinen, T., Schobesberger, S., Kangasluoma, J., Kontkanen, J., Nieminen, T., Kurtén, T., Nielsen, L. B., Jørgensen, S., Kjaergaard, H. G., Canagaratna, M., Maso, M. D., Berndt, T., Petäjä, T., Wahner, A., Kerminen, V. M., Kulmala, M., Worsnop, D. R., Wildt, J. and Mentel, T. F.: A large source of low-volatility secondary organic aerosol, Nature, 506(7489), 476–479, doi:10.1038/nature13032, 2014.

Fuzzi, S., Andreae, M. O., Huebert, B. J., Kulmala, M., Bond, T. C., Boy, M., Doherty, S. J., Guenther, A., Kanakidou, M., Kawamura, K., Kerminen, V. M., Lohmann, U., Russell, L. M. and Pöschl, U.: Critical assessment of the current state of scientific knowledge, terminology, and research needs concerning the role of organic aerosols in the atmosphere, climate, and global change, Atmos. Chem. Phys., 6(7), 2017–2038, doi:10.5194/acp-6-2017-2006, 2006.

Galeazzo, T., Valorso, R., Li, Y., Camredon, M., Aumont, B. and Shiraiwa, M.: Estimation of secondary organic aerosol viscosity from explicit modeling of gas-phase oxidation of isoprene and α-pinene, Atmos. Chem. Phys., 21(13), 10199–10213, doi:10.5194/acp-21-10199-2021, 2021.

Gao, Y., Chen, S. B. and Yu, L. E.: Efflorescence relative humidity for ammonium sulfate particles, J. Phys. Chem. A, 110(24), 7602–7608, doi:10.1021/jp057574g, 2006.

Gkatzelis, G. I., Hohaus, T., Tillmann, R., Gensch, I., Müller, M., Eichler, P., Xu, K. M., Schlag, P. H., Schmitt, S., Yu, Z., Wegener, R., Kaminski, M., Holzinger, R., Wisthaler, A. and Kiendler-Scharr, A.: Gas-to-particle partitioning of major biogenic oxidation products: A study on freshly formed and aged biogenic SOA, Atmos. Chem. Phys., 18(17), 12969–12989, doi:10.5194/acp-18-12969-2018, 2018.

Hallquist, M., Wenger, J. C., Baltensperger, U., Rudich, Y., Simpson, D., Claeys, M., Dommen, J., Donahue, N. M., George, C., Goldstein, A. H., Hamilton, J. F., Herrmann, H., Hoffmann, T., Iinuma, Y., Jang, M., Jenkin, M. E., Jimenez, J. L., Kiendler-Scharr, A., Maenhaut, W., McFiggans, G., Mentel, T. F., Monod, A., Prévôt, A. S. H., Seinfeld, J. H., Surratt, J. D., Szmigielski, R. and Wildt, J.: The formation, properties and impact of secondary organic aerosol: Current and emerging issues, Atmos. Chem. Phys., 9(14), 5155–5236, doi:10.5194/acp-9-5155-2009, 2009.

Hsiao, T. C., Young, L. H., Tai, Y. C. and Chen, K. C.: Aqueous film formation on irregularly shaped inorganic nanoparticles before deliquescence, as revealed by a hygroscopic differential mobility analyzer–Aerosol particle mass system, Aerosol Sci. Technol., 50(6), 568–577, doi:10.1080/02786826.2016.1168512, 2016.

Jia, L. and Xu, Y. F.: The role of functional groups in the understanding of secondary organic aerosol formation mechanism from α-pinene, Sci. Total Environ., 738, 139831, doi:10.1016/j.scitotenv.2020.139831, 2020.

Jimenez, J. L., Canagaratna, M. R., Donahue, N. M., Prevot, A. S. H., Zhang, Q., Kroll, J. H., DeCarlo, P. F., Allan, J. D., Coe, H., Ng, N. L., Aiken, A. C., Docherty, K. S., Ulbrich, I. M., Grieshop, A. P., Robinson, A. L., Duplissy, J., Smith, J. D., Wilson, K. R., Lanz, V. A., Hueglin, C., Sun, Y. L., Tian, J., Laaksonen, A., Raatikainen, T., Rautiainen, J., Vaattovaara, P., Ehn, M., Kulmala, M., Tomlinson, J. M., Collins, D. R., Cubison, M. J., Dunlea, E. J., Huffman, J. A., Onasch, T. B., Alfarra, M. R., Williams, P. I., Bower, K., Kondo, Y., Schneider, J., Drewnick, F., Borrmann, S., Weimer, S., Demerjian, K., Salcedo, D., Cottrell, L., Griffin, R., Takami, A., Miyoshi, T., Hatakeyama, S., Shimono, A., Sun, J. Y., Zhang, Y. M., Dzepina, K., Kimmel, J. R., Sueper, D., Jayne, J. T., Herndon, S. C., Trimborn, A. M., Williams, L. R., Wood, E. C., Middlebrook, A. M., Kolb, C. E., Baltensperger, U. and Worsnop, D. R.: Evolution of organic aerosols in the atmosphere, Science (80-.)., 326(5959), 1525–1529, doi:10.1126/science.1180353, 2009.

Johnson, J. S., Regayre, L. A., Yoshioka, M., Pringle, K. J., Lee, L. A., Sexton, D. M. H., Rostron, J. W., Booth, B. B. B. and Carslaw, K. S.: The importance of comprehensive parameter sampling and multiple observations for robust constraint of aerosol radiative forcing, Atmos. Chem. Phys., 18(17), 13031–13053, doi:10.5194/acp-18-13031-2018, 2018.

Khamaganov, V. G. and Hites, R. A.: Rate constants for the gas-phase reactions of ozone with isoprene, α- and β-pinene, and limonene as a function of temperature, J. Phys. Chem. A, 105(5), 815–822, doi:10.1021/jp002730z, 2001.

Krasnomowitz, J. M., Apsokardu, M. J., Stangl, C. M., Tiszenekel, L., Ouyang, Q., Lee, S. and Johnston, M. V.: Growth of

Aitken Mode Ammonium Sulfate Particles by α-Pinene Ozonolysis, Aerosol Sci. Technol., 53(4), 1–14, doi:10.1080/02786826.2019.1568381, 2019.

Lehtipalo, K., Yan, C., Dada, L., Bianchi, F., Xiao, M., Wagner, R., Stolzenburg, D., Ahonen, L. R., Amorim, A., Baccarini, A., Bauer, P. S., Baumgartner, B., Bergen, A., Bernhammer, A. K., Breitenlechner, M., Brilke, S., Buchholz, A., Mazon, S. B., Chen, D., Chen, X., Dias, A., Dommen, J., Draper, D. C., Duplissy, J., Ehn, M., Finkenzeller, H., Fischer, L., Frege, C., Fuchs, C., Garmash, O., Gordon, H., Hakala, J., He, X., Heikkinen, L., Heinritzi, M., Helm, J. C., Hofbauer, V., Hoyle, C. R., Jokinen, T., Kangasluoma, J., Kerminen, V. M., Kim, C., Kirkby, J., Kontkanen, J., Kürten, A., Lawler, M. J., Mai, H., Mathot, S., Mauldin, R. L., Molteni, U., Nichman, L., Nie, W., Nieminen, T., Ojdanic, A., Onnela, A., Passananti, M., Petäjä, T., Piel, F., Pospisilova, V., Quéléver, L. L. J., Rissanen, M. P., Rose, C., Sarnela, N., Schallhart, S., Schuchmann, S., Sengupta, K., Simon, M., Sipilä, M., Tauber, C., Tomé, A., Tröstl, J., Väisänen, O., Vogel, A. L., Volkamer, R., Wagner, A. C., Wang, M., Weitz, L., Wimmer, D., Ye, P., Ylisirniö, A., Zha, Q., Carslaw, K. S., Curtius, J., Donahue, N. M., Flagan, R. C., Hansel, A., Riipinen, I., Virtanen, A., Winkler, P. M., Baltensperger, U., Kulmala, M. and Worsnop, D. R.: Multicomponent new particle formation from sulfuric acid, ammonia, and biogenic vapors, Sci. Adv., 4(12), 1–10, doi:10.1126/sciadv.aau5363, 2018.

Mertes, P., Pfaffenberger, L., Dommen, J., Kalberer, M. and Baltensperger, U.: Development of a sensitive long path absorption photometer to quantify peroxides in aerosol particles (Peroxide-LOPAP), Atmos. Meas. Tech., 5(10), 2339–2348, doi:10.5194/amt-5-2339-2012, 2012.

Najjar, Y. S. H.: Gaseous Pollutants Formation and Their Harmful Effects on Health and Environment, Innov. Energy Policies, 1(January 2011), 1–9, doi:10.4303/iep/e101203, 2011.

Pathak, R. K., Presto, A. A., Lane, T. E., Stanier, C. O., Donahue, N. M. and Pandis, S. N.: Ozonolysis of α-pinene: Parameterization of secondary organic aerosol mass fraction, Atmos. Chem. Phys., 7(14), 3811–3821, doi:10.5194/acp-7-3811-2007, 2007a.

Pathak, R. K., Stanier, C. O., Donahue, N. M. and Pandis, S. N.: Ozonolysis of α-pinene at atmospherically relevant concentrations: Temperature dependence of aerosol mass fractions (yields), J. Geophys. Res. Atmos., 112(3), 1–8, doi:10.1029/2006JD007436, 2007b.

Pierce, J. R. and Adams, P. J.: Efficiency of cloud condensation nuclei formation from ultrafine particles, Atmos. Chem. Phys., 7(5), 1367–1379, doi:10.5194/acp-7-1367-2007, 2007.

Riipinen, I., Pierce, J. R., Yli-Juuti, T., Nieminen, T., Häkkinen, S., Ehn, M., Junninen, H., Lehtipalo, K., Petäjä, T., Slowik, J., Chang, R., Shantz, N. C., Abbatt, J., Leaitch, W. R., Kerminen, V. M., Worsnop, D. R., Pandis, S. N., Donahue, N. M. and Kulmala, M.: Organic condensation: A vital link connecting aerosol formation to cloud condensation nuclei (CCN) concentrations, Atmos. Chem. Phys., 11(8), 3865–3878, doi:10.5194/acp-11-3865-2011, 2011.

Saha, P. K. and Grieshop, A. P.: Exploring Divergent Volatility Properties from Yield and Thermodenuder Measurements of Secondary Organic Aerosol from α-Pinene Ozonolysis, Environ. Sci. Technol., 50(11), 5740–5749, doi:10.1021/acs.est.6b00303, 2016.

Sarnela, N., Jokinen, T., Duplissy, J., Yan, C., Nieminen, T., Ehn, M., Schobesberger, S., Heinritzi, M., Ehrhart, S., Lehtipalo,

K., Tröstl, J., Simon, M., Kürten, A., Leiminger, M., Lawler, M. J., Rissanen, M. P., Bianchi, F., Praplan, A. P., Hakala, J., Amorim, A., Gonin, M., Hansel, A., Kirkby, J., Dommen, J., Curtius, J., Smith, J. N., Petäjä, T., Worsnop, D. R., Kulmala, M., Donahue, N. M. and Sipilä, M.: Measurement-model comparison of stabilized Criegee intermediate and highly oxygenated molecule production in the CLOUD chamber, Atmos. Chem. Phys., 18(4), 2363–2380, doi:10.5194/acp-18-2363-2018, 2018.

Shrivastava, M., Cappa, C. D., Fan, J., Goldstein, A. H., Guenther, A. B., Jimenez, J. L., Kuang, C., Laskin, A., Martin, S. T., Ng, N. L., Petaja, T., Pierce, J. R., Rasch, P. J., Roldin, P., Seinfeld, J. H., Shilling, J., Smith, J. N., Thornton, J. A., Volkamer, R., Wang, J., Worsnop, D. R., Zaveri, R. A., Zelenyuk, A. and Zhang, Q.: Recent advances in understanding secondary organic aerosol: Implications for global climate forcing, Rev. Geophys., 55(2), 509–559, doi:10.1002/2016RG000540, 2017.

Smith, G. D., Woods, E., DeForest, C. L., Baer, T. and Miller, R. E.: Reactive uptake of ozone by oleic acid aerosol particles: Application of single-particle mass spectrometry to heterogeneous reaction kinetics, J. Phys. Chem. A, 106(35), 8085–8095, doi:10.1021/jp020527t, 2002.

Stangl, C. M., Krasnomowitz, J. M., Apsokardu, M. J., Tiszenkel, L., Ouyang, Q., Lee, S. and Johnston, M. V.: Sulfur Dioxide Modifies Aerosol Particle Formation and Growth by Ozonolysis of Monoterpenes and Isoprene, J. Geophys. Res. Atmos., 124(8), 2018JD030064, doi:10.1029/2018JD030064, 2019.

Stanier, C. O., Pathak, R. K. and Pandis, S. N.: Measurements of the volatility of aerosols from α-pinene ozonolysis, Environ. Sci. Technol., 41(8), 2756–2763, doi:10.1021/es0519280, 2007.

Thompson, J. E.: Airborne Particulate Matter: Human Exposure and Health Effects, J. Occup. Environ. Med., 60(5), 392–423, doi:10.1097/JOM.0000000000001277, 2018.

Tolocka, M. P., Jang, M., Ginter, J. M., Cox, F. J., Kamens, R. M. and Johnston, M. V.: Formation of Oligomers in Secondary Organic Aerosol, Environ. Sci. Technol., 38(5), 1428–1434, doi:10.1021/es035030r, 2004a.

Tolocka, M. P., Saul, T. D. and Johnston, M. V.: Reactive Uptake of Nitric Acid into Aqueous Sodium Chloride Droplets Using Real-Time Single-Particle Mass Spectrometry, J. Phys. Chem. A, 108(14), 2659–2665, doi:10.1021/jp036612y, 2004b.

Trump, E. R. and Donahue, N. M.: Oligomer formation within secondary organic aerosols: Equilibrium and dynamic considerations, Atmos. Chem. Phys., 14(7), 3691–3701, doi:10.5194/acp-14-3691-2014, 2014.

Vestenius, M., Hellén, H., Levula, J., Kuronen, P., Helminen, K. J., Nieminen, T., Kulmala, M. and Hakola, H.: Acidic reaction products of monoterpenes and sesquiterpenes in atmospheric fine particles in a boreal forest, Atmos. Chem. Phys., 14(15), 7883–7893, doi:10.5194/acp-14-7883-2014, 2014.

Xavier, C., Rusanen, A., Zhou, P., Dean, C., Pichelstorfer, L., Roldin, P. and Boy, M.: Aerosol mass yields of selected biogenic volatile organic compounds - a theoretical study with nearly explicit gas-phase chemistry, Atmos. Chem. Phys. Discuss., 1–26, doi:10.5194/acp-2019-424, 2019.

Zaveri, R. A., Shilling, J. E., Zelenyuk, A., Liu, J., Bell, D. M., D'Ambro, E. L., Gaston, C. J., Thornton, J. A., Laskin, A., Lin, P., Wilson, J., Easter, R. C., Wang, J., Bertram, A. K., Martin, S. T., Seinfeld, J. H. and Worsnop, D. R.: Growth Kinetics and Size Distribution Dynamics of Viscous Secondary Organic Aerosol, Environ. Sci. Technol., 52(3), 1191–1199, doi:10.1021/acs.est.7b04623, 2018.

Zaveri, R. A., Shilling, J. E., Zelenyuk, A., Zawadowicz, M. A., Suski, K., China, S., Bell, D. M., Veghte, D. and Laskin, A.: Particle-Phase Diffusion Modulates Partitioning of Semivolatile Organic Compounds to Aged Secondary Organic Aerosol, Environ. Sci. Technol., 54(5), 2595–2605, doi:10.1021/acs.est.9b05514, 2020.

Zhang, D. and Zhang, R.: Ozonolysis of α -pinene and B -pinene: Kinetics and mechanism, J. Chem. Phys., 122(11), doi:10.1063/1.1862616, 2005.

Zhang, X., McVay, R. C., Huang, D. D., Dalleska, N. F., Aumont, B., Flagan, R. C. and Seinfeld, J. H.: Formation and evolution of molecular products in α-pinene secondary organic aerosol, Proc. Natl. Acad. Sci. U. S. A., 112(46), 14168–14173, doi:10.1073/pnas.1517742112, 2015.

Zhou, S., Rivera-Rios, J. C., Keutsch, F. N. and Abbatt, J. P. D.: Identification of organic hydroperoxides and peroxy acids using atmospheric pressure chemical ionization-tandem mass spectrometry (APCI-MS/MS): Application to secondary organic aerosol, Atmos. Meas. Tech., 11(5), 3081–3089, doi:10.5194/amt-11-3081-2018, 2018.

Zhu, J. and Penner, J. E.: Global Modeling of Secondary Organic Aerosol With Organic Nucleation, J. Geophys. Res. Atmos., 124(14), 8260–8286, doi:10.1029/2019JD030414, 2019.

Ziemann, P. J. and Atkinson, R.: Kinetics, products, and mechanisms of secondary organic aerosol formation, Chem. Soc. Rev., 41(19), 6582–6605, doi:10.1039/c2cs35122f, 2012.

Page 8: [1] Deleted Johnston, Murray 7/13/22 12:12:00 PM

Page 8: [1] Deleted Johnston, Murray 7/13/22 12:12:00 PM

Page 8: [2] Deleted Johnston, Murray 7/13/22 12:12:00 PM

Page 8: [2] Deleted Johnston, Murray 7/13/22 12:12:00 PM

Page 8: [2] Deleted Johnston, Murray 7/13/22 12:12:00 PM

Page 8: [3] Deleted Johnston, Murray 7/13/22 12:12:00 PM

Page 8: [3] Deleted Johnston, Murray 7/13/22 12:12:00 PM

Page 8: [4] Deleted Johnston, Murray 7/13/22 12:12:00 PM

Page 8: [4] Deleted Johnston, Murray 7/13/22 12:12:00 PM

Page 8: [5] Deleted Johnston, Murray 7/13/22 12:12:00 PM

Page 8: [6] Deleted Johnston, Murray 7/13/22 12:12:00 PM

Page 8: [6] Deleted Johnston, Murray 7/13/22 12:12:00 PM

Page 8: [6] Deleted Johnston, Murray 7/13/22 12:12:00 PM

Page 8: [7] Deleted Johnston, Murray 7/13/22 12:12:00 PM

Page 8: [7] Deleted Johnston, Murray 7/13/22 12:12:00 PM

Page 8: [8] Deleted Johnston, Murray 7/13/22 12:12:00 PM

Page 8: [8] Deleted Johnston, Murray 7/13/22 12:12:00 PM

Page 8: [8] Deleted Johnston, Murray 7/13/22 12:12:00 PM

Page 8: [9] Deleted Johnston, Murray 7/13/22 12:12:00 PM

Page 8: [9] Deleted Johnston, Murray 7/13/22 12:12:00 PM

Page 8: [9] Deleted	**Johnston, Murray**	**7/13/22 12:12:00 PM**
Page 8: [9] Deleted	**Johnston, Murray**	**7/13/22 12:12:00 PM**
Page 8: [10] Deleted	**Johnston, Murray**	**7/13/22 12:12:00 PM**
Page 9: [11] Deleted	**Johnston, Murray**	**7/13/22 12:12:00 PM**
Page 9: [12] Deleted	**Johnston, Murray**	**7/13/22 12:12:00 PM**
Page 9: [13] Deleted	**Johnston, Murray**	**7/13/22 12:12:00 PM**
Page 9: [14] Deleted	**Johnston, Murray**	**7/13/22 12:12:00 PM**
Page 9: [15] Deleted	**Johnston, Murray**	**7/13/22 12:12:00 PM**
Page 9: [16] Deleted	**Johnston, Murray**	**7/13/22 12:12:00 PM**
Page 9: [17] Deleted	**Johnston, Murray**	**7/13/22 12:12:00 PM**
Page 11: [18] Deleted	**Johnston, Murray**	**7/13/22 12:12:00 PM**
Page 15: [19] Deleted	**Johnston, Murray**	**7/13/22 12:12:00 PM**
Page 15: [20] Deleted	**Johnston, Murray**	**7/13/22 12:12:00 PM**